Journal of The Electrochemical Society, **152** (8) A1682-A1693 (2005)
0013-4651/2005/152(8)/A1682/12/$7.00 © The Electrochemical Society, Inc.

A Mathematical Model for a Lithium-Ion Battery/Electrochemical Capacitor Hybrid System

Godfrey Sikha,* Ralph E. White, and Branko N. Popov***,z**

Department of Chemical Engineering, University of South Carolina, Columbia, South Carolina 29208, USA

A one-dimensional model for predicting the performance of a battery/electrochemical capacitor-hybrid system has been developed. Simulation results are presented for a $LiCoO_2|LiPF_6$ ethylene carbonate/dimethyl carbonate|carbon battery system and a Maxwell PC 10F carbon double-layer electrochemical capacitor. The current shared between the battery and the electrochemical capacitor at very short times depends on the ohmic resistances of the battery and the capacitor. As the discharge proceeds, the operating conditions such as frequency, duty ratio, and peak pulse discharge current control the current shared among parallel circuits. These parameters also determine the extent of the run time increase of the hybrid system as compared to the battery system. The inclusion of a number of identical series/parallel capacitors is considered in the present model by introducing the parameter, capacitor configuration index. Ragone plots are simulated for a battery-alone and a hybrid system. A substantial improvement in the available energy density is observed while operating hybrid systems under high power densities. Finally, a general optimization approach is presented.
 [DOI: 10.1149/1.1940749]

Manuscript submitted October 25, 2004; revised manuscript received February 14, 2005. Available electronically July 14, 2005.

Electrochemical double-layer capacitors are the most suitable power source for high-powered applications such as electric vehicles, power distribution systems, uninterrupted power supply, hybrid vehicles and other electronic devices due to their high power densities.[1,2] However, their energy densities are considerably lower than those of high-energy battery systems such as lithium ion. Although advanced battery systems and double-layer electrochemical capacitors contrast with regard to energy-power relationship, in combination they can be utilized as an effective power source. In several experimental studies, hybrid systems with batteries and capacitors have been demonstrated to extend the run time and improve the power capability of the battery.[3,4] However, there has not yet been a rigorous theoretical analysis on this subject. Dougal et al.[5] presented analytical solutions to a simplified model of a battery-capacitor hybrid system based on circuit modeling and discussed in detail the energy efficiency, power capabilities, and current sharing between the battery and the capacitor. However, a more systematic study on an electrochemical basis is required to understand the processes occurring in the battery-capacitor hybrid system in order to evaluate and improve the performance.

The objective of this paper is to develop a more sophisticated macrohomogenous model to simulate the performance of a battery-electrochemical capacitor hybrid system and to analyze the improvement in performance compared to that of battery-alone systems under high-current pulse loads. Pulse loads were typically chosen because they are frequently encountered in portable power systems such as machine guns, implantable cardioverter defribillators, electric vehicles and in wireless telecommunication systems. The model addresses the effect of pulse operating conditions, specifically the duty ratio, pulse frequency, and the pulse current amplitude on the performance of the hybrid system. In addition, the model has been used to simulate the effect of the capacitor configuration index (the ratio of the number of capacitors in parallel to the number of capacitors in series) on the performance of the hybrid system. Finally, energy-power relations for hybrid systems are compared with battery systems as such and on a mass basis for different operating conditions.

Numerous models have been published which predict the performance of either a lithium-ion battery or a supercapacitor. For the case of supercapacitors, the double-layer charging phenomenon was first modeled by Posey and Morozumi et al.[6] However the performance of a double-layer electrochemical capacitor was studied in detail by Pillay and Newman[7] only in the mid-1990s. Later Srinivasan and Weidner[8] presented an analytical solution for the performance of a double-layer capacitor under constant current operation. More advanced models[9,10] for electrochemical capacitors that include pseudocapacitance (in which the energy storage mechanism is due to faradaic reaction) along with double-layer charging have been studied in detail for different systems. Similarly, a mathematical model for a lithium-ion battery using porous electrode theory[11,12] and concentrated solution theory[13] was first developed by Doyle et al.[14] for a solid lithium anode and a porous cathode. Later Fuller et al.[15] extended the model to a lithium-ion battery with two porous electrodes.

None of these models was used to study the performance of a battery-capacitor network. Ong and Newman[16] simulated the performance of a dual lithium-ion insertion cell with the inclusion of the double-layer capacitance of the battery and studied the transient potential response at very short times. In the present work, a hybrid network with an electrochemical capacitor in parallel with a battery is simulated for pulse current discharges. The goal is to understand the effect of the addition of capacitors in parallel to the battery and analyze the improvements in run time extension, utilization, energy and power enhancement.

Model Development

Assumptions.— The model system considered in this work has a lithium-ion battery in parallel with an electrochemical double-layer capacitor network, represented by a single capacitor with an effective capacitance, as shown in Fig. 1. The battery consists of a porous $LiCoO_2$ cathode and a LiC_6 anode with small amounts of binder and conductive material. The electrodes are sandwiched using a polypropylene separator, which is ionically conducting but electronically insulating, filled with 1 M $LiPF_6$ in an EC/DMC mixture. The electrochemical capacitor (shown in the lower part of Fig. 1) has three regions with two identical porous carbon electrodes that act as anode and cathode, separated by an ionically conductive separator. The current distribution in the current collectors is ignored in both the capacitor and the battery and hence the ends of the anode and cathode act as boundaries. The assumptions made in the battery part of the hybrid model are summarized as: (*i*) The model is one dimensional; (*ii*) D and t^+ are constant with respect to concentration; (*iii*) temperature effects within the cell are ignored; (*iv*) volume changes associated within the cell are ignored and hence constant porosities are considered; and (*v*) for the solid phase diffusion, instead of solving the spherical diffusion rigorously, a polynomial approximation of the concentration is considered.[17,18] For the case of the electrochemical capacitor, the following assumptions are made: (*i*) one-dimensional, constant transport properties in the solution phase; (*ii*) pseudocapacitance is neglected and the energy storage mechanism is

* Electrochemical Society Student Member.
** Electrochemical Society Fellow.
*** Electrochemical Society Active Member.
z E-mail: popov@engr.sc.edu

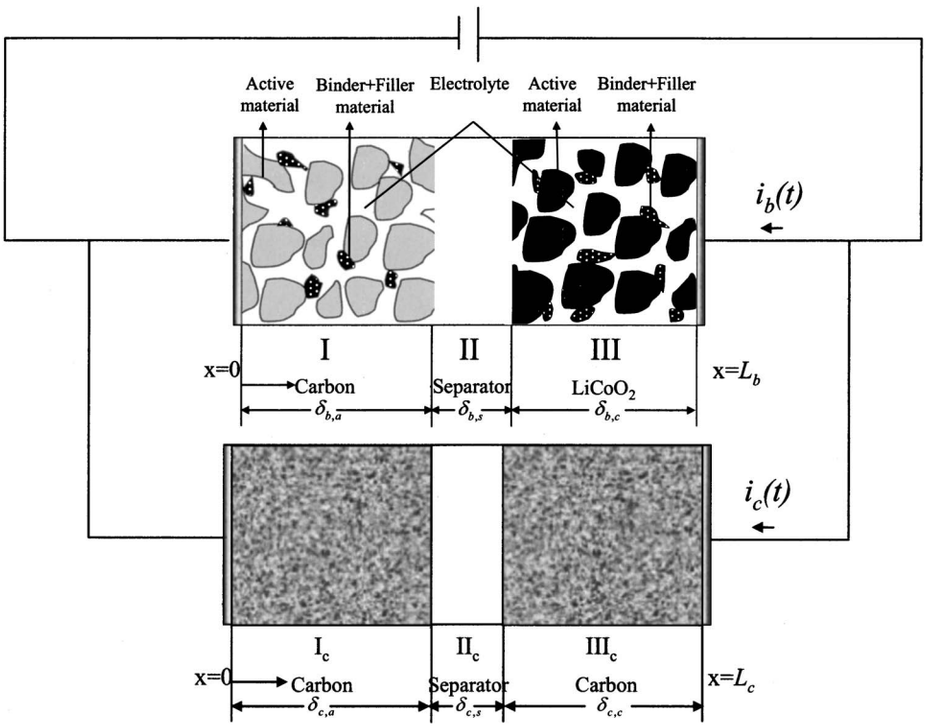

Figure 1. Schematic of a lithium-ion battery/electrochemical capacitor network hybrid system. The battery consisted of a positive $LiCoO_2$ and negative carbon electrode with a separator while the electrochemical capacitor has carbon electrodes as anode and cathode sandwiched against a separator.

completely due to the charging of the double layer; and (*iii*) temperature changes within the cell are ignored. The applied current, i.e., the load in the external circuit, is shared between the battery and the capacitor based on the resistances across either network

Governing equations.— The governing equations for the battery closely follow those of Doyle et al. and are discussed in detail elsewhere.[14,15] The solution phase mass balance for the Li^+ in the electrolyte is

$$\frac{\partial(\varepsilon_{b,j}c_b)}{\partial t} = \frac{\partial}{\partial x}\left(D_{b,j}^{eff}\frac{\partial c_b}{\partial x}\right) + \frac{a_{b,j}\, j_{n,b,j}(1 - t_{b,+}^0)}{\tilde{\upsilon}_b^+} - \left(t_{b,+}^0\frac{d\tilde{q}_{b-}}{d\tilde{q}_b} - t_{b,-}^0\frac{d\tilde{q}_{b+}}{d\tilde{q}_b}\right)\frac{t_{b,+}^0 a_{b,j}C_{b,dl}}{F\tilde{\upsilon}_{b,+}} \times\left\{\frac{\partial}{\partial t}(\phi_{1,b,j} - \phi_{2,b,j})\right\}, \quad j = n,p \qquad [1]$$

Note that $(d\tilde{q}_{b+}/d\tilde{q}_b) = 1$ and $(d\tilde{q}_{b-}/d\tilde{q}_b) = 0$ for a cation adsorbing electrode and $(d\tilde{q}_{b+}/d\tilde{q}_b) = 0$ and $(d\tilde{q}_{b-}/d\tilde{q}_b) = 1$ for an anion adsorbing electrode.[19]

The current densities in the solid matrix ($\mathbf{i}_{1,b,j}$) and the solution phase ($\mathbf{i}_{2,b,j}$) are given by Ohm's law

$$\mathbf{i}_{1,b,j} = -\sigma_{b,j}^{eff}\nabla\phi_{1,b,j}, \quad j = n,p \qquad [2]$$

$$\mathbf{i}_{2,b,j} = -\kappa_b^{eff}\left\{\nabla\phi_{2,b,j} - \frac{2RT}{F}\left(1 + \frac{\partial \ln f}{\partial \ln c_b}\right)(1 - t_{b,+}^0)\nabla \ln c_b\right\} \quad j = n,p \qquad [3]$$

The relationship between the divergence of the current flow and the reaction rate is expressed as

$$\nabla\cdot\mathbf{i}_{2,b,j} = -\frac{n}{s_i}Fa_{b,j}j_{n,b,j} + a_{b,j}C_{b,dl}\left\{\frac{\partial}{\partial t}(\phi_{1,b,j} - \phi_{2,b,j})\right\} \quad j = n,p \qquad [4]$$

The current that flows through the matrix or the solution phase is conserved and it leads to the equation

$$\mathbf{i}_{1,b,j} + \mathbf{i}_{2,b,j} = i_b(t) \qquad [5]$$

Here the sum of the solid phase current density and the solution phase current density is a function of time and is an unknown that has to be determined. In the case of galvanostatic charging, this is equal to the applied current; however, in this case the value of $i_b(t)$ can be determined only by considering the capacitor network, which is discussed later.

The solid phase diffusion of the inserted lithium into the active material is governed by the Fick's law for diffusion

$$\frac{\partial c_{s,j}}{\partial t} = \frac{1}{r^2}\frac{\partial}{\partial r}\left(D_{s,j}r^2\left(\frac{\partial c_{s,j}}{\partial r}\right)\right) \quad j = n,p \qquad [6]$$

where r is the direction normal to the surface of the particle.

Finally, the intercalation kinetics in either electrode is written in the form of Butler-Volmer expressions with concentration-dependent exchange current density. The kinetics for such a charge-transfer reaction is given by

$$j_{n,j} = k_j(c_b)^{\alpha_{a,j}}(c_{T,j} - c_{s,j})^{\alpha_{a,j}}(c_{s,j})^{\alpha_{c,j}}\left\{\exp\left(\frac{\alpha_{a,j}F}{RT}(\eta_j)\right) - \exp\left(\frac{-\alpha_{c,j}F}{RT}(\eta_j)\right)\right\}, \quad j = n,p \qquad [7]$$

where

$$\eta_j = \phi_{1,b,j} - \phi_{2,b,j} - U_j, \quad j = n,p \qquad [8]$$

and U_j is a function of solid phase concentration which is measured experimentally at low rates and the expression is included in Appendix A.

For the capacitor network the mass balance on the salt including the double-layer charging yields

$$\frac{\partial(\varepsilon_{c,j}c_c)}{\partial t} = \frac{\partial}{\partial x}\left(D_{c,j}^{eff}\frac{\partial c_c}{\partial x}\right) - \left(t_{c,+}^0\frac{d\tilde{q}_{c-}}{d\tilde{q}_c} - t_{c,-}^0\frac{d\tilde{q}_{c,+}}{d\tilde{q}_c}\right)\frac{a_{c,j}C_{c,dl}}{F\tilde{\upsilon}_{c,+}}\left\{\frac{\partial}{\partial t}(\phi_{1,c,j} - \phi_{2,c,j})\right\}, \quad j = n,p \qquad [9]$$

Here, too, $(d\tilde{q}_{c+}/d\tilde{q}_c) = 1$ and $(d\tilde{q}_{c-}/d\tilde{q}_c) = 0$ for a cation adsorbing (negative) electrode and $(d\tilde{q}_{c+}/d\tilde{q}_c) = 0$ and $(d\tilde{q}_{c-}/d\tilde{q}_c) = 1$ for an anion adsorbing (positive) electrode. The current densities in the solid matrix ($\mathbf{i}_{1,c,j}$) and the solution phase ($\mathbf{i}_{2,c,j}$) are given by

$$\mathbf{i}_{1,c,j} = -\sigma_{c,j}^{eff}\nabla\phi_{1,c,j}, \quad j = n,p \qquad [10]$$

$$\mathbf{i}_{2,c,j} = -\kappa_c^{eff}\left\{\nabla\phi_{2,c,j} - \frac{2RT}{F}(1 - t_{c,+}^o)\nabla\ln c_c\right\} \quad j = n,p \qquad [11]$$

for an ideal solution, and the relationship between the divergence of the current flow and the reaction rate in the capacitor is expressed as

$$\nabla\cdot\mathbf{i}_{2,c,j} = a_{c,j}C_{c,dl}\left\{\frac{\partial}{\partial t}(\phi_{1,c,j} - \phi_{2,c,j})\right\} \quad j = n,p \qquad [12]$$

All the current that crosses the interface ultimately charges the double layer because the occurrence of any faradaic reaction is ignored.

In the capacitor, also, the conservation of charge leads to

$$\mathbf{i}_{1,c,j} + \mathbf{i}_{2,c,j} = i_c(t) \qquad [13]$$

Here $i_c(t)$ is the current density discharged from the capacitor, which is a function of time. However, we know that the external current withdrawn from the hybrid system should be either from the capacitor or the battery and hence

$$A_b i_b(t) + A_c i_c(t) = I_{app} \qquad [14]$$

The fourteen dependent variables to be solved for are c_b, $\mathbf{i}_{1,b}$, $\mathbf{i}_{2,b}$, $\phi_{1,b}$, $\phi_{2,b}$, $j_{n,j}$, c_s, $i_b(t)$, c_c, $\mathbf{i}_{1,c}$, $\mathbf{i}_{2,c}$, $\phi_{1,c}$, $\phi_{2,c}$, and $i_c(t)$. Equations 1-14, except Eq. 8, constitute 13 governing equations, one for each variable defined. The final relation necessary to make the system of equations completely solvable is obtained by applying Kirchoff's law in the closed circuit containing the battery and capacitor network, resulting in the condition that the potential across the battery and the capacitor network equals each other and is also equal to the cell potential, V_{cell}. Mathematically this can be written as

$$\phi_{1,b}|_{x=L_b} - \phi_{1,b}|_{x=0} = n_s(\phi_{1,c}|_{x=L_c} - \phi_{1,c}|_{x=0}) = V_{cell} \qquad [15]$$

The boundary conditions for solving the equations in the battery are discussed in detail in Ref. 15 and 20, while those for the capacitor are discussed in Ref. 8-10.

The model is simulated for a pulse discharge current with a current amplitude I_p, duty ratio ψ, frequency υ, and time period $T(1/\upsilon)$. The current function can be written as

$$\left.\begin{aligned} I_{app} &= I_p, \quad 0 < t \leq \frac{N+\psi}{\upsilon} \\ I_{app} &= 0, \quad t > \frac{N+\psi}{\upsilon} \end{aligned}\right\} \qquad [16]$$

where N is the number of pulses elapsed at time t and I_p is the peak current.

The addition of capacitors to the battery is simulated by assuming that the current shared by each capacitor is the same. Thus if identical capacitors are added in parallel or in series, the effective current to a capacitor can be calculated and used in the model. The parameter, capacitor configuration index (Λ), which is defined as the ratio of the number of capacitors in parallel, n_p, to the number of capacitors in series, n_s, controls the effective current to each capacitor. As a result, Eq. 14 takes the form

Table I. Electrode parameter values for the lithium-ion battery.[a]

Parameters	LiC_6	$LiCoO_2$	Source
Electrode parameters			
$D_s(m^2/s)$	3.89×10^{-14}	1×10^{-13}	a
$\sigma_b(S/m)$	100	100	a
$c_T(mol/m^3)$	30555	51554	e
$C_{b,dl}(F/m^2)$	0.2	0.2	Ref. 16
$\rho_b(kg/m^3)$	5031.67	2291.62	e
$\delta_b(1/\sigma_b^{eff} + 1/\kappa_b^{eff})(\Omega m^2)$	1.115×10^{-2}	5.539×10^{-3}	e
$a_b C_{b,dl}\delta_b^2(1/\sigma_b^{eff} + 1/\kappa_b^{eff})(ms)$	29.82	18.72	e
$\tilde{R}_b(\Omega)$	0.173		e
Thermodynamic and kinetic parameters			
k	4.92×10^{-10}	1.39×10^{-10}	i
α_c	0.5	0.5	a
α_a	0.5	0.5	a
Design adjustable parameters			
ε_b	0.31	0.39	a
ε_b^f	0.5	0.12	a
$R_s(m)$	12.5×10^{-6}	8×10^{-6}	a
$brug_b$	3.3	3.3	a
δ_b	87×10^{-6}	92×10^{-6}	m
$l_b(m)$	0.462	0.465	m
$b_b(m)$	0.055	0.053	m
Δy	0.9	0.53	m
$m_b(g)$	42.86		m

[a] i-Evaluated at initial conditions, m-measured from Sony US 18650 1.5 Ah cells, a-assumed values, e-estimated values.

$$A_b i_b(t) + n_s\Lambda A_c i_c(t) = I_{app} \qquad [17]$$

where $i_c(t)$ is the current flowing through each capacitor.

Model parameters and solution method.— The parameter values used for the battery in the model are listed in Tables I and II, while the parameters for the electrochemical capacitor are listed in Table III. The open-circuit potentials of the positive and negative electrodes are measured at a very low rate in a T-cell setup with a pure lithium foil as a reference/counter electrode; the expressions are given in Appendix A. The parameter values for the transport properties in solution and the design parameters for the battery used in simulation were based on a Sony US18650 cell (1.5 Ah) with $LiCoO_2$ cathode, carbon anode, polypropylene separator, and ethylene carbonate (EC)/dimethyl carbonate (DMC)/$LiPF_6$ electrolyte. For the case of the electrochemical capacitor, the parameters were taken from a Maxwell PC 10F capacitor (2.5 V), which has a carbon anode and cathode and an organic electrolyte (acetonitrile). The capacitor configuration index, Λ (ratio of the number of capacitors in parallel to the number of capacitors in series), was varied by chang-

Table II. Electrolyte and separator parameter values for the lithium-ion battery.[a]

Parameter	Value	Source
$D_b(m^2/s)$	7.5×10^{-10}	Ref. 27
$c_b^0(mol/m^3)$	1000	a
$t_{b,+}^0$	0.373	a
n	1	e
f	1	a
$T(K)$	298	a
ε_b^s	0.723	a
$brug_b^s$	0	a
δ_b^s	22×10^{-6}	m

[a] i-Evaluated at initial conditions, m-measured (Sony US 18650 1.5 Ah cells), a-assumed values, e-estimated values.

Table III. Parameter value for the electrochemical capacitor.[a]

Parameters	Carbon electrode	Source
σ_b(S/m)	100	a
$C_{c,dl}$(F/m^2)	0.2	e
ε_c	0.38	Ref. 9
ε_c^f	0.5	a
$Brug_c$	1.5	a
$Brug_c^s$	0	a
$\hat{R}_c$(m)	1×10^{-8}	Ref. 9
δ_c^a, δ_c^c(m)	3.76×10^{-4}	m
ε_c^s	0.7	Ref. 9
κ_c(S/m)	5	Ref. 28
c_c^0(mol/m^3)	200	a
D_c(m^2/s)	1.8×10^{-9}	a
$t_{c,+}^0$	0.814	a
δ_c^s(m)	0.52×10^{-4}	m
l_c(m)	7×10^{-2}	m
b_c(m)	2.3×10^{-2}	m
m_c(g)	0.4861	m
$\widetilde{R}_c(\Omega)$	0.070	e
$a_c C_{c,dl} \delta_c^2 (1/\sigma_c^{eff} + 1/\kappa_c^{eff})$(s)	4.217	e

[a] m-Measured [Maxwell PC 10F capacitor (2.5 V)] capacitor: a-assumed values, e-estimated values.

ing the value of n_p, while the value of n_s was always set to 2. This is because the capacitor has a completely charged potential of 2.5 V while the battery has a potential of 4.2 V, and hence, by coupling two capacitors in series the voltage balance can approximately be set initially. The solid phase diffusion within the spherical particle in the battery is solved by considering a parabolic profile for the solid phase concentration so as to make the problem one-dimensional (Appendix C). The spatial variables were cast into a three-point finite difference scheme and the resulting differential algebraic equations were solved using the subroutine DASSL in FORTRAN.

Results and Discussion

Figure 2a shows the comparison of the voltage profile of a battery and a battery-capacitor hybrid under a pulse load. The capacitance of the capacitor corresponding to a configuration index of 0.5 is taken to be 0.1 F/m^2. The amplitude of the pulse, I_p, was 4.178 A, which corresponds to 3 C rate, where C represents the capacity of the battery (the capacity of the capacitor was neglected). The duty ratio ψ for the pulse current is 0.1 and the frequency υ is 1 Hz. Due to the high ohmic resistance in the battery, the ohmic potential drop in the battery was much higher than in the hybrid system, wherein the effective resistance was decreased by the parallel capacitor network. The ohmic voltage drop in the case of the battery was around 0.2612 V, while the hybrid system showed a voltage drop of only 0.1024 V. Hence, the presence of the capacitor brings out the voltage drop gradually. This drastic reduction in the ohmic drop is very beneficial for the increase in the utilization of the battery. The utilization of the battery, ξ, is defined as the ratio of the capacity q extracted from the battery using a particular discharge protocol to the theoretical capacity q_{max}. After the initial drop, the voltage profile of the battery-alone system depends on the pulse amplitude and the relation of the open-circuit potential on the state of charge of the battery. However, in the case of the hybrid system the potential profile is determined by the discharge of the capacitor as well. The potential drop for the hybrid system during on time (after the ohmic drop) is higher (0.0565 V) than observed for the battery system (0.0017 V). This is because in the hybrid system, at the start of the pulse, the capacitor takes up the major current and then progressively the battery shares the major part of the current while the capacitor loses out its capacity at a faster rate. Thus, instead of an

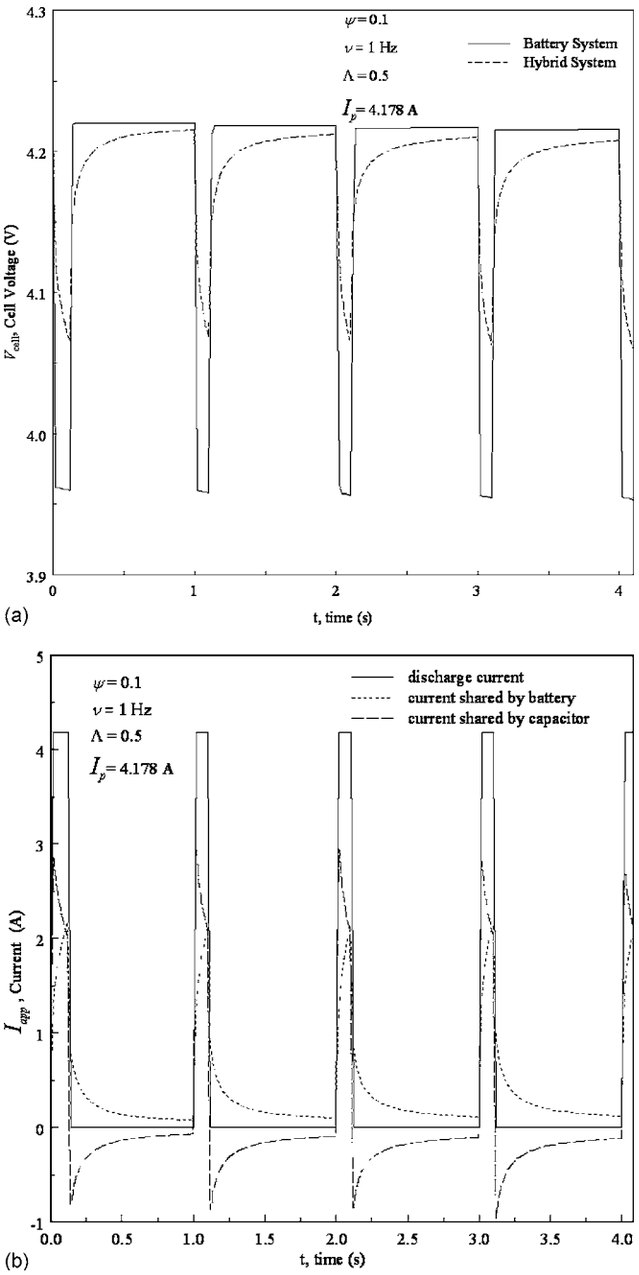

Figure 2. (a) Comparison of cell voltages for the battery and the hybrid system for short times. (b) Current shared by the battery and the capacitor for short times. Simulation results are for the case where $\psi = 0.1$ and $\upsilon = 1$ Hz.

instantaneous pulse a series of small-step pulses with increasing amplitudes is effected on the battery in the hybrid system. As a consequence, a sudden drop in the potential is not observed in the hybrid system; however, as the current to the battery in the hybrid system increases it induces additional ohmic drop, and hence, the potential drop during the on time of the pulse is higher in the case of the hybrid system. In the battery-alone system, once the initial resistance induces a potential drop further potential changes are only due to polarization because the current to the battery is constant during the on time of the pulse. During the off time of the pulse, the battery immediately regains the potential drop due to the ohmic resistances. The transient potential profile of the hybrid is slightly

different from that of the battery; the hybrid needs a longer time to come back to equilibrium, which depends on the time constant of the capacitor.

The transient current shared between the capacitor and the battery in a hybrid system for the same set of operating parameters can be simulated using the model, as shown in Fig. 2b. As discussed above, due to the high ohmic resistance of the battery as compared to capacitor, the major part of the current initially passes through the capacitor network and a small part through the battery. However, during the on time of the pulse the current shared by the battery increases with time while the current in the capacitor network decreases within a certain pulse. The rate of increase of the current in the battery is determined by the effective capacitance of the capacitor. Once the current is switched off in the external circuit (off time of the pulse) the battery would recharge the capacitor in the hybrid system, as seen from the negative currents in the capacitor in Fig. 2b. This is because while the battery and the capacitor maintain the same potential during the on time of the pulse, the effect of the ohmic resistance is greater in the battery than the capacitor, and hence when the current in the external circuit is switched off the battery naturally shoots up to a higher potential than the capacitor. However, the potential across the battery and the capacitor should be the same during the off time also and in the process of maintaining the potential the battery recharges the capacitor. Thus, even in the case when the current in the external circuit is zero there is a current within the battery capacitor circuit, as seen in Fig. 2b (the dotted line and the dashed line). This is also the reason for the slower transience in the voltage profile during the off time of the pulse in the hybrid system as compared to the battery system, seen in Fig. 2a.

Another important feature to be noted is that the recharging current from the battery (Fig. 2b) does not decay to zero during the off time. This is because the potentials across the capacitor and the battery are balanced with the inclusion of the potential drop due to the ohmic resistances. Only when the open-circuit potentials of both the capacitor and the battery are equal will the current in the battery hybrid circuit reduce to zero; this is determined by the time constant of the hybrid system given approximately by $(\widetilde{R}_b + \widetilde{R}_c)\widetilde{C}_c$, where $\widetilde{R}_b$ and $\widetilde{R}_c$ are the total internal dc resistances of the battery and the capacitor network, respectively. The time taken for the decay of the current during the off time of the Nth pulse is approximately determined from Eq. 18, which is derived from a circuit network (Appendix B)

$$i_c(t) = i_c^{max} \exp\left(-\frac{t}{(\widetilde{R}_b + \widetilde{R}_c)\widetilde{C}_c}\right), \quad \frac{N+\psi}{\upsilon} < t < \frac{N+1}{\upsilon} \quad [18]$$

$$i_c^{max} = \frac{t}{(\widetilde{R}_b + \widetilde{R}_c)\widetilde{C}_c}\int_0^{t=N+\psi/\upsilon} i_c(t)dt \quad [19]$$

Thus, at $\psi = 0.1$ and $\upsilon = 1$ Hz the off time is not sufficient to restore the battery and capacitor components to equilibrium. This negatively impacts the performance of the hybrid system because the next pulse follows before complete relaxation of the voltage profile and hence, the run time becomes shorter. However, this is specific to the system chosen, and the time needed to restore the capacitor to equilibrium (which is more important) could vary largely based on the response time of the electrochemical capacitor chosen. The inherent time constants for the capacitor and the battery network are evaluated through the expressions $a_b C_{b,dl}\delta_b^2(1/\sigma_b^{eff} + 1/\kappa_b^{eff})$ and $a_c C_{c,dl}\delta_b^2(1/\sigma_c^{eff} + 1/\kappa_c^{eff})$ respectively.

Figure 3a compares the voltage profile of the battery and the hybrid system at a higher duty ratio ($\psi = 0.8$) and at the same frequency ($\upsilon = 1$ Hz). Here the potential drop during the on time of the pulse for the hybrid system is much higher (0.1212 V) than in the case where $\psi = 0.1$. In addition, because the off time is much shorter, the relaxation of the potential transience is much less and thus a high duty ratio may not be favorable for an extended run time.

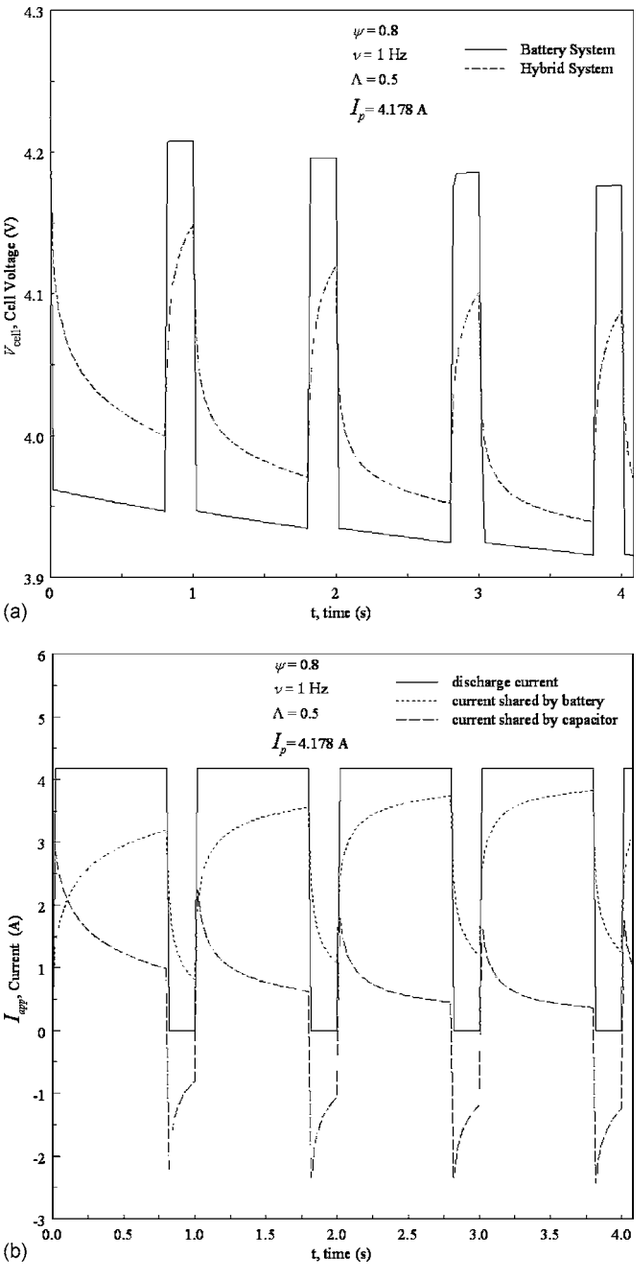

Figure 3. (a) Comparison of cell voltages for the battery and the hybrid system for short times. (b) Current shared by the battery and the capacitor for short times. Simulation results are for the case where $\psi = 0.8$ and $\upsilon = 1$ Hz.

The current shared between the battery and the capacitor for this operating condition is shown in Fig. 3b. At high duty ratios the current drawn from the battery dominates because the current that can be withdrawn from the capacitor network is limited by its effective capacitance. By the end of the on time in the first pulse the capacitor loses most of its energy, and once the off time of the pulse starts, a huge negative current is drawn by the capacitor, indicating that the battery is charging the almost completely utilized capacitor. However, since the off time is shorter at higher duty ratios the battery is not able to charge the capacitor completely. This is reflected in the next pulse (Fig. 3b), where the battery current dominates the capacitor shortly after the on time of the pulse, and in the subsequent pulses the battery supplies most of the current to the external

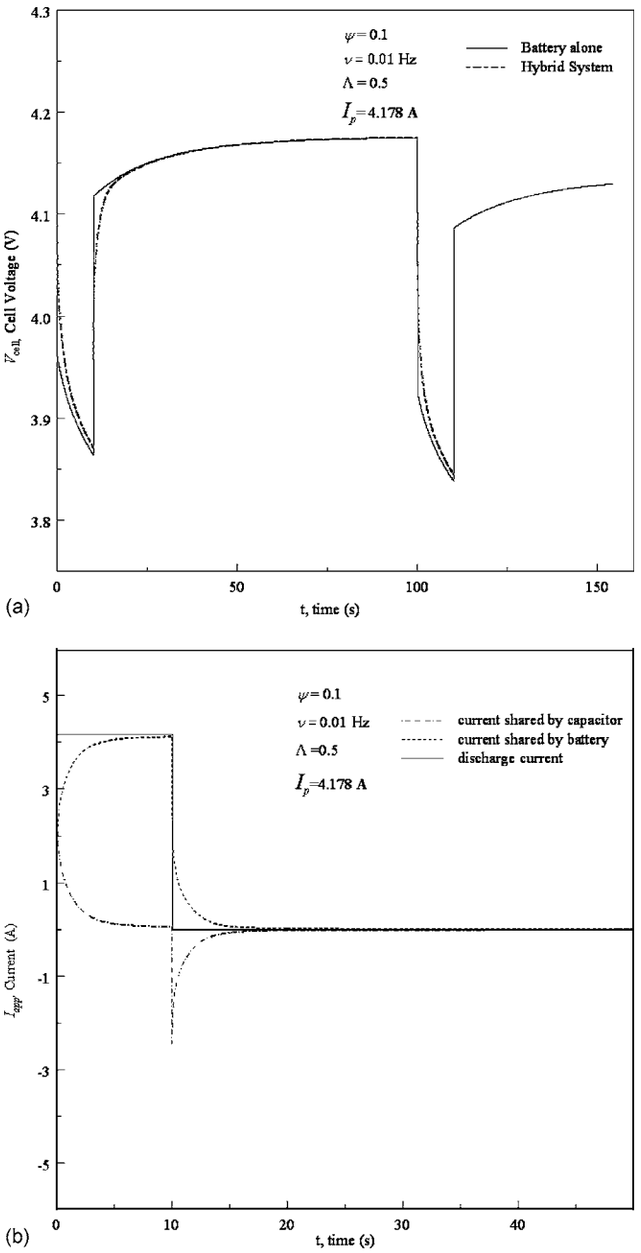

Figure 4. (a) Comparison of cell voltages for the battery and the hybrid system for short times. (b) Current shared by the battery and the capacitor for short times. Simulation results are for the case where $\psi = 0.1$ and $\nu = 0.01$ Hz.

circuit right from the start of the on time of the pulse. This will also inhibit the smooth transition of potential profiles at a later stage and the hybrid system will start behaving like a battery suppressing the utility of the capacitor.

At low frequencies ($\upsilon < 0.01$) the presence of a capacitor in the hybrid system makes no significant difference and the potential profiles are very similar to those of the battery-alone system. This can be seen in Fig. 4a, where the potential profiles of the battery and the hybrid system overlap almost completely. Subsequently, the off time of the pulse is also larger and hence a complete relaxation back to equilibrium is established, as seen in Fig. 4b, because the current during the off time of the pulse decays to zero based on Eq. 18 and the open-circuit potentials of both the battery and the capacitor become equal. The time for which the capacitor in the hybrid has an effect on the discharge curve depends on the time constant of the limiting component in the hybrid. The inherent time constants for the battery calculated through $\tilde{\tau}_b = a_b C_{b,dl} L_b^2 (1/\sigma_b^{eff} + 1/\kappa_b^{eff})$ is evaluated to be a much lesser value as compared to the time constant of the electrochemical capacitors, given by $\tilde{\tau}_c = a_c C_{c,dl} L_c^2 (1/\sigma_c^{eff} + 1/\kappa_c^{eff})$, thereby making the time constant of the capacitor a dominating factor in determining the time beyond which the discharge curves of the battery and the battery/electrochemical capacitor almost follow the same path.

A sufficient off time is necessary for high current pulses for the effective utilization of the battery, and hence the duty ratio, ψ, is an important parameter. The concentration gradients established during the on time of the pulse must be sufficiently relaxed during the off time so that the salt concentration is not depleted anywhere within the cell. The relaxation time also allows redistribution of the intercalated lithium more evenly inside the active material, thereby improving the utilization. Figure 5a shows the relaxation of the dimensionless concentration, $\bar{c}_b$, in the battery during the off time of the pulse for a cell simulated with a pulse amplitude $I_p = 4.178$ A, $\psi = 0.1$, and $\upsilon = 0.01$ Hz. Because $\upsilon = 0.01$ and $\psi = 0.1$, after 10 s of on time the off time of the pulse starts. The concentration profiles at 8 s (during on time) and 90 s (during off time) show the effect of concentration relaxation. Once again, when the next pulse is delivered the concentration profiles show steep gradients ($t = 110$ s). Figure 5b shows the dimensionless salt concentration distribution in the capacitor for the same conditions described above. It can be seen that the net concentration of salt in the solution increases while the capacitor is discharged and while charging back, the capacitor loses the concentration in the solution to the interface, thereby contributing to the double-layer charge. The concentration has a distinct profile in the positive electrode when compared to the negative because of the higher cation transference number. Figure 6a compares the discharge curves obtained by simulating a battery and a hybrid system with a capacitor configuration index, $\Lambda = 0.5$, $I_p = 4.178$ A, $\psi = 0.5$, and $\upsilon = 1$ Hz. This figure clearly indicates the decreased ohmic drop of the hybrid system (indicated by circles) as compared to the battery system (indicated by diamonds). The figure also captures the increase in the run time of the hybrid system over the battery system. Figure 6b shows the potential profile of the battery and the hybrid system more clearly. The diamond symbols at the top connect to the bottom diamond symbols through gray lines during the pulse switch from off to on, and the reverse happens when the current is switched from on to off. In the case of the hybrid the dark lines connect the circle symbols. Due to the presence of the capacitor in the hybrid system, an abrupt drop in the potential was eliminated.

The performance analysis was done under high-current pulse discharges based on complete discharge of the battery/hybrid system from a fully charged state to a cutoff potential of 2.5 V. Figure 7 compares the utilization of the battery, ξ, in the battery-alone system and the hybrid system. The capacity, q, extracted from the pure battery system can be calculated directly from the product of the pulse amplitude I_p, duty ratio ψ, and the run time τ, while the capacity extracted from the battery in the hybrid system is estimated by numerically integrating the current density from the battery, i_b, over the run time τ of the hybrid system. The utilization of the battery in the hybrid system is thus calculated using the formula

$$\xi = \frac{1}{q_{max}} \int_0^{\tau} A_b i_b(t) dt \qquad [20]$$

Each point in Fig. 7 is obtained by running the battery/hybrid system under a pulse amplitude $I_p = 4.178$ A with a specific value of duty ratio and frequency until a cutoff potential of 2.5 V. The dashed lines represent the utilization of the battery-alone system while the continuous lines represent the utilization of the battery in the hybrid system. It can be inferred that high frequencies and low duty ratios

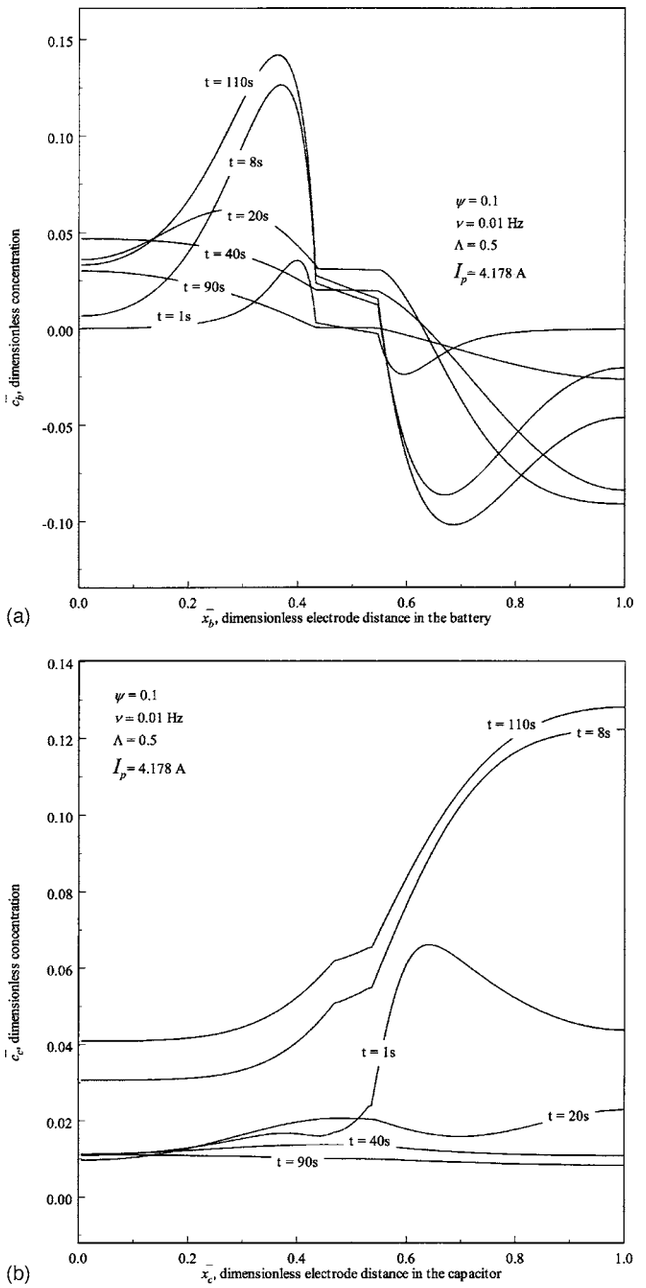

Figure 5. (a) Plot showing the concentration relaxation phenomenon in the (a) battery and (b) electrochemical capacitor during pulse discharge. Lines correspond to the dimensionless concentration profiles during the on time/off time of the pulse with the time marked on the curves.

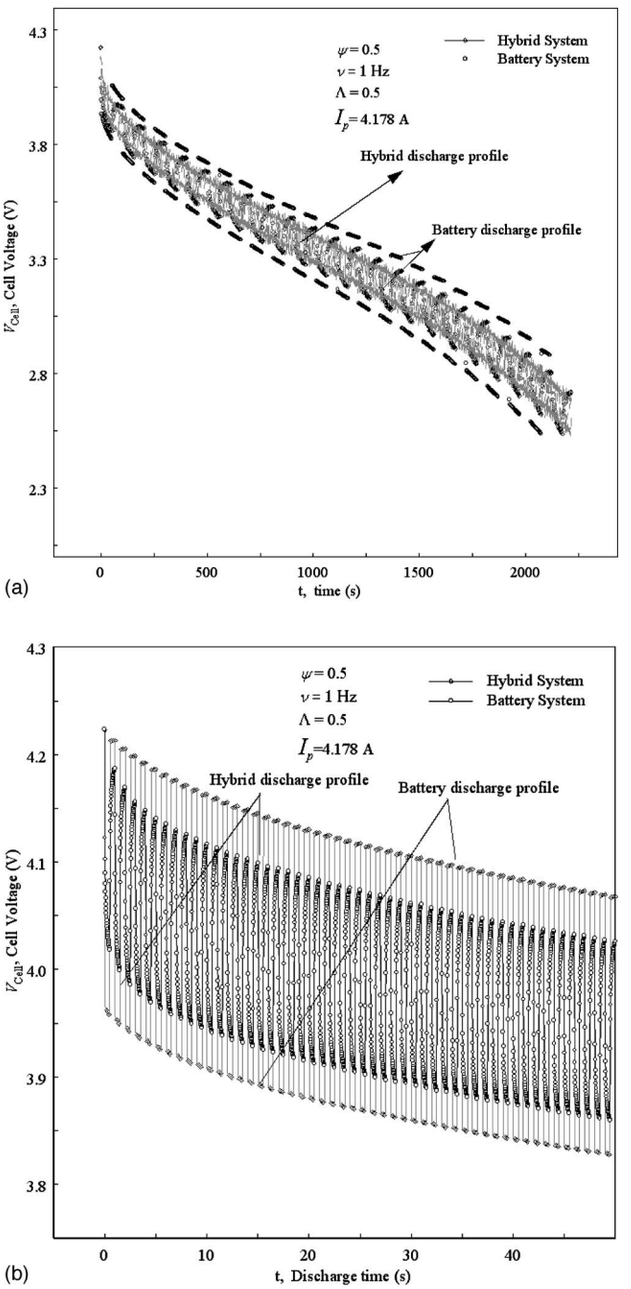

Figure 6. (a) Discharge curve for the pure battery system and hybrid system which shows the reduced voltage drop and the increased run time for the hybrid system as compared to the battery system. (b) Discharge curve for the pure battery system and hybrid system at short times. Simulated results are for the case $\psi = 0.5$ and $\upsilon = 1$ Hz.

yield better utilization of the battery. This is a common feature in both the battery-alone system and the battery in the hybrid system. This figure also reveals a substantial increase in the utilization of the battery in the hybrid system over the battery alone system.

The run time extension of the hybrid system, which is defined as the ratio of the increase in the run time of the hybrid system over that of the battery system to the run time of the hybrid, is plotted against the duty ratio for varying frequencies in Fig. 8. The simulated results show that the run time extension increases with the increase in pulse frequency over the entire range of duty ratios. However, for a given frequency ($\upsilon = 0.01$ Hz), the run time extension peaks at around $\psi = 0.2$, and with the increase in frequency the peak shifts toward higher duty ratios. This is in close agreement with the experimental results reported by Sikha and Popov.[21] When the limit ψ tends to zero the run time $\tau \rightarrow \infty$ and hence the run time extension is theoretically zero. When $\psi \rightarrow 1$, the run times of the battery and the hybrid system are almost the same except for a small increase in run time of the hybrid system due to the discharge of the capacitor, which occurs during the initial part of the discharge. This increase is proportional to the time constant of the capacitor and hence depends on the effective capacitance of the capacitor network.

Figure 9 shows the power enhancement factor λ, which is defined as the ratio of the average power delivered by the hybrid

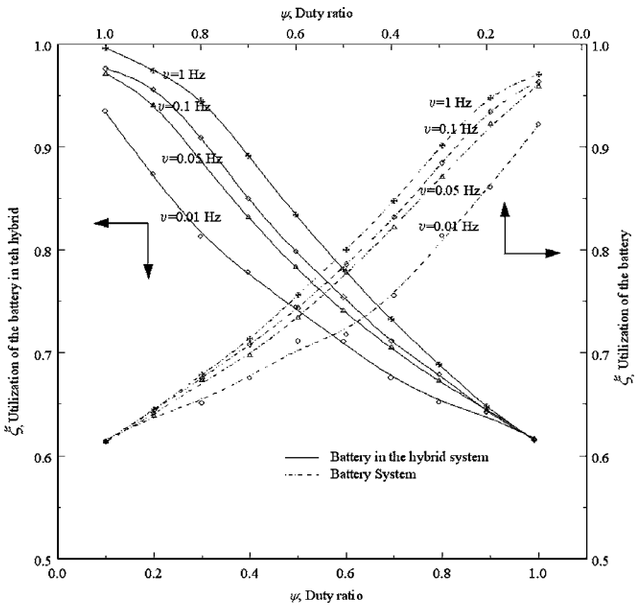

Figure 7. Plot showing the effect of duty ratio (ψ) on the utilization (ξ) of the pure battery and the battery in the hybrid system for various values of frequencies. The simulations are done for a current amplitude of I_p = 4.178 A.

system to the average power delivered by the battery under the same discharge protocol. The average power is calculated based on the time during which the pulse was active and is given by

$$P_{ave} = \frac{1}{\tau\psi}\int_0^{\tau} I_{app}V_c dt \qquad [21]$$

where $\int_0^{\tau} I_{app}V_c dt$ is the total energy withdrawn from the system. The average power is found to be inversely proportional to the duty ratio. The values of the power enhancement factor are always greater than unity. This suggests that although the hybrid system sustains a longer run time, which effectively diminishes the value of $1/\tau\psi$, the average power is higher than that of the battery-alone system. This is because of a much higher voltage regime of the hybrid system during discharge as compared to the battery-alone system (Fig. 6b).

Effect of capacitor configuration index (Λ).— The number of capacitors added to the battery to make up the hybrid system is very crucial in determining the performance of the hybrid system. While the addition of capacitors improves the performance of the battery, the addition of capacitors adds to the mass of the hybrid system, which could possibly decrease the energy and power densities of the system. Simulations on the effect of the capacitor configuration index allow analysis of the increment in the energy/power delivered with the increment of mass to the system through the addition of capacitors in parallel or series. In this work all the simulations are based on a single battery and capacitors are added in different proportions to alter the value of the capacitor configuration index. Furthermore, because we use a Li-ion battery (which has a voltage range of 2.5-4.2 V) and a Maxwell electrochemical capacitor (which has a voltage range of 0-2.5 V), the number of capacitors in series is fixed at two so as to match the voltage of the battery for a fully charged hybrid system. Adding more than two capacitors in series would cause overcharging conditions on the battery when the capacitors get fully charged, and adding less than two could cause the capacitor to be overcharged by the battery, i.e., go over the limit of 2.5 V, beyond which solvent oxidation could reduce the current efficiency of the electrochemical capacitor. However, the addition of capacitors in parallel is beneficial in increasing the performance of the battery due to the increase in the effective capacitance. The effective capacitance, $\tilde{C}_c^{eff}$, when a string of n_s capacitors in series are connected in parallel with n_p capacitors is given by

$$\frac{1}{\tilde{C}_c^{eff}} = \frac{1}{n_p}\sum_{i=1}^{n_s}\frac{1}{\tilde{C}_{c,i}^{eff}} = \frac{1}{\Lambda\tilde{C}_c}(\textit{if identical}) \qquad [22]$$

In this work all the capacitors are assumed to be identical in nature. For the capacitors in series configuration, the current entering the individual capacitor is the same while the net potential is the summation of the potential across each capacitor, and for the parallel configuration the current entering is shared equally based on the number of parallel circuits, while the net potential remains the same across each capacitor. Thus it is realistic to use Eq. 17 when simulating for different capacitor configuration indices, making the computation easier for any number of identical capacitors.

Figure 10 shows the variation of utilization of the battery ξ in a hybrid system with pulse amplitude (I_p) for different values of the capacitor configuration index, Λ. Simulations were done for fixed values of ψ = 0.5 and υ = 0.1 Hz. The results clearly demonstrate the improvement in the rate capability of the battery in the hybrid system with the increase in Λ. For the battery-alone system, the utilization is close to unity only at a very low rate, close to 0.6963 A (~2 h rate). Such poor utilization is enhanced by the addition of capacitors in parallel. The simulations presented in Fig. 10 reveal that for the hybrid system where Λ is high, the maximum utilization of the battery can be achieved even at much higher discharge rates (~1/4 h rate), which is commonly encountered in high-power applications. At high pulse discharge rates, it is difficult to extract the active material completely for two major reasons: (*i*) diffusion limitations in the solid and solution phases may deplete the available lithium species at regions of high reaction rate within the cell, and (*ii*) when higher current causes higher ohmic drop, the time to reach the cutoff potential during discharge becomes much shorter. The addition of capacitors to the system decreases the ohmic drop because the effective resistance is reduced. In addition, for hybrid systems with higher capacitor configuration index the current shared

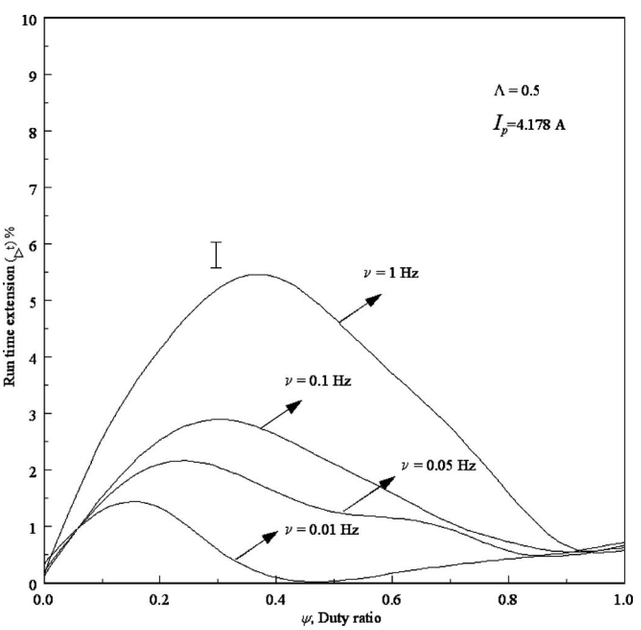

Figure 8. Simulated values of the percentage increase in the run time of the hybrid system over that of the battery system for different values of duty ratio. The effect of frequency on the run time extension of the hybrid system is also shown. The simulations are done for a current amplitude of I_p = 4.178 A and discharged to 2.5 V.

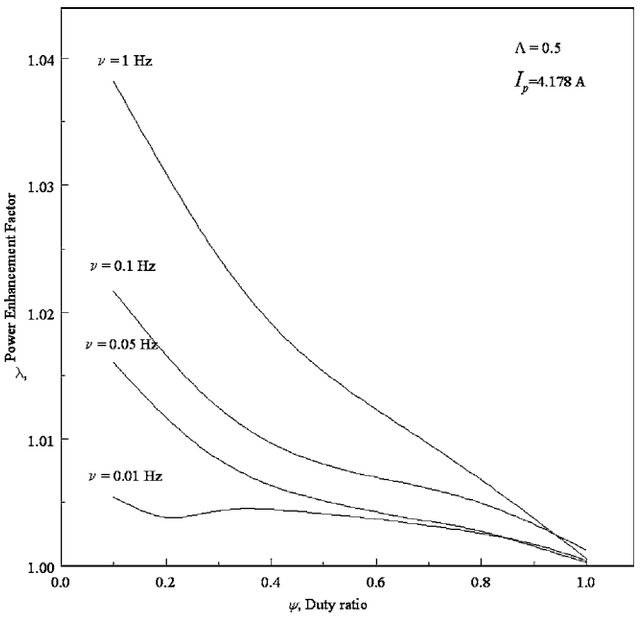

Figure 9. Power enhancement factor as a function of duty ratio. The effect of frequency on the power enhancement factor was also simulated. All simulations were done at $I_p = 4.178$ A and capacitor configuration index $\Lambda = 0.5$.

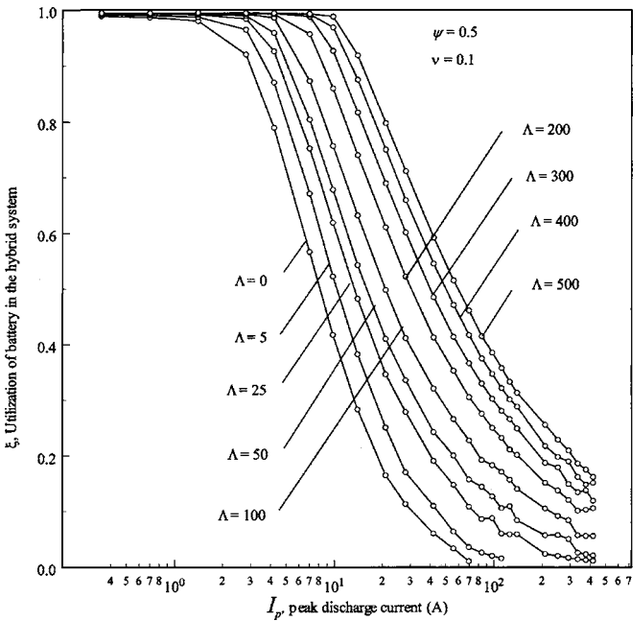

Figure 10. Simulated utilization of the battery as a function of discharge rate (peak pulse discharge current density). The plot also shows the better rate capability (high utilization at higher rates) at higher values of capacitor configuration index.

by the battery decreases, which in turn decreases the diffusion limitations in the cell and improves the utilization of the battery. This can also be explained using the time constant of the hybrid system as estimated through Eq. 18, where in the approximate time constant when the capacitance in the battery is neglected it is estimated to be $(\tilde{R}_b + \tilde{R}_c)\tilde{C}_c$. Thus, for a string of capacitors with a configuration index of Λ the net time constant would be $(\tilde{R}_b + \tilde{R}_c/\Lambda)\tilde{C}_c\Lambda$, which keeps the time constant increasing with the increase in Λ and hence at high values of Λ the effect of the capacitor is seen in the hybrid system for a longer period of time, making the utilization of the battery better.

Figure 11a shows the simulated relationship between the available energy and the corresponding average power delivered for various values of configuration index, Λ. Each point on the curve is obtained by running the discharge curve until the cutoff potential of 2.5 V at a particular pulse amplitude I_p with fixed values of $\psi = 0.5$ and $\upsilon = 0.1$ Hz. This plot supplies useful information on the optimization of the number of capacitors to be added to the battery for a certain application. In the case of low-power demands ($\sim$10 W), a slight increase in the number of coupled capacitors will not be very useful because the increase in energy is not substantial, whereas for high-power demands ($\sim$200 W) the increase in energy is significant even when relatively few capacitors are coupled to the battery. However, for the optimization of energy and power, taking the mass of the system into consideration, the plot of power density (W/kg) against the energy density (Wh/kg), the Ragone plot (Fig. 11b) is critical. The mass (m) of the hybrid system, calculated by taking into account the mass of the active material, current collector, electrolyte, and conductive filler for both the battery and the capacitor, is given by

$$m = \left\{ \begin{array}{l} A_b \sum_{j=n,s,p} \delta_{b,j}[\rho_{b,j}(1 - \varepsilon_{b,j} - \varepsilon^f_{b,j}) + \rho^l_{b,j}\varepsilon_{b,j} + \rho^f_{b,j}\varepsilon^f_{b,j}] \\ + n_s^2 \Lambda A_c \sum_{j=n,s,p} \delta_{c,j}[\rho_{c,j}(1 - \varepsilon_{c,j} - \varepsilon^f_{c,j}) + \rho^l_{c,j}\varepsilon_{c,j} + \rho^f_{c,j}\varepsilon^f_{c,j}] \end{array} \right\} \quad [23]$$

The term $n_s^2\Lambda$ accounts for the total number of the capacitors; in the present study, since the number of capacitors in series is fixed at 2, this term takes a value of 4Λ, where A_b and A_c are the surface area of the battery and the capacitor, respectively, when the electrodes are unwound. The mass of the insulating cover and the can are ignored in the calculation of the total mass. Previous research[22] has shown that a power density of 200 W/kg can be obtained for Sony 18650 cells at 2 C rate (constant current) with an associated energy density loss of about 60% of the nominal value (obtained through a low-rate discharge). From the Ragone plots shown in Fig. 11b, one can infer that a power density of $\sim$300 W/kg can be obtained for a battery-alone system through a pulse discharge protocol with $\psi = 0.5$ and $\upsilon = 0.1$ Hz, and the associated energy loss from the nominal value is less than 25%. The nominal value of the simulated energy for a pure battery is 120.8 Wh/kg, which is close to the reported values for $LiCoO_2$/carbon systems.[23,24] The Ragone plots present crucial information regarding the hybrid system; it is observed that for low power densities, the hybrid system with higher configuration index predicts much lower energy densities than that of the battery-alone system. However, for the hybrid system with high configuration index, where the number of capacitors is large, the trade-off between the mass of the system and the power density becomes crucial. For higher power densities the energy density predicted for the hybrid system with high configuration index is better than that for the battery-alone system. This is an important consideration in the design aspects of a hybrid system.

Optimization.— A scheme for optimization largely depends on the actual requirements of a specific application. If we assume that the discharge time of the hybrid system is the main optimization to be considered when the capacitor configuration index is kept low ($\Lambda < 10$), the Ragone plots reveal that for low values of capacitor configuration index there is no significant difference in energy density between the battery and the hybrid system. Thus, ignoring the effect of adding mass to the system for low values of Λ, the operation frequency and duty ratio can be targeted for maximum run time. The analysis shown in Fig. 8 gives more insight about how to alter

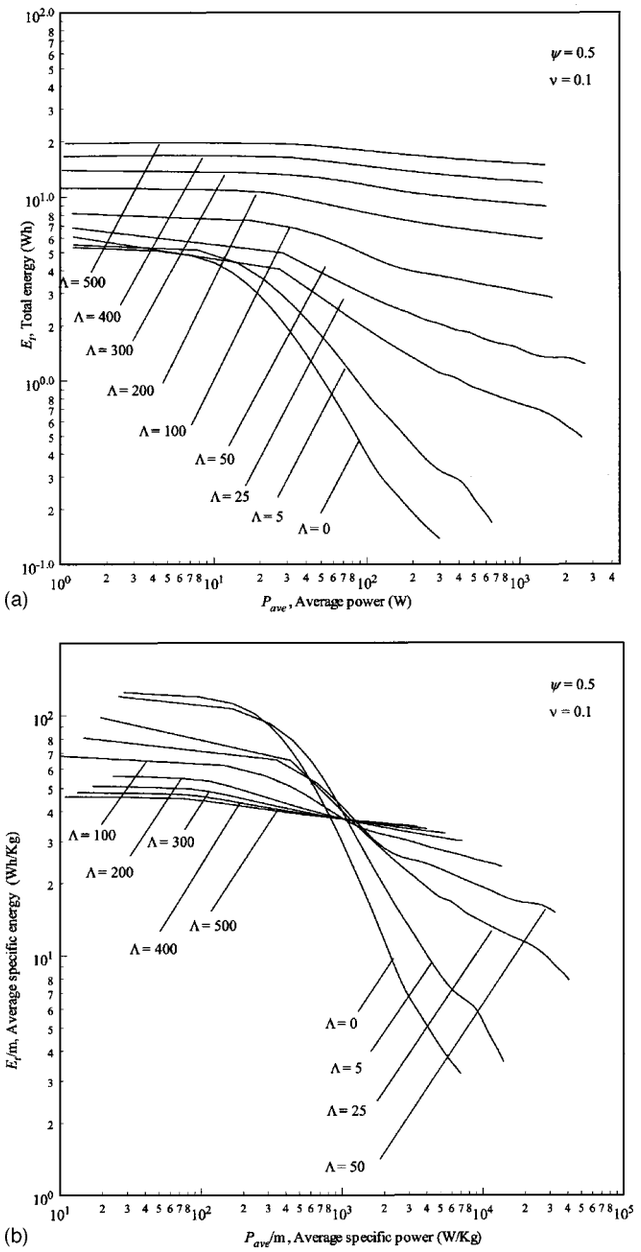

Figure 11. (a) Plot showing the total energy (E_t) vs average power relationship for various values of capacitor configuration index, Λ. Each point on the curve was obtained by running the hybrid model at different pulse discharge rates. (b) Ragone plot comparison for the battery and hybrid system for various values of capacitor configuration index. This figure shows the improvement in the energy-delivering capacity of the hybrid system under high-power operations.

the duty ratio based on the frequency of pulse operation or vice versa. Another optimization consideration would be to extract maximum utilization of the battery at a faster rate. In such a case the effect of the pulse discharge current I_p on the utilization should be analyzed based on the information supplied in Fig. 10. When the hybrid system is designed to obtain high power and energy, then the capacitor configuration index is an important parameter that must be optimized; Fig. 11b gives information regarding such optimization. It can be inferred from Fig. 11b, while operating under lower average power requirements, higher capacitor configuration index is disadvantageous; however, for high-power requirements the energy densities obtained from hybrid systems with higher capacitor index are much better than the battery system. This is a crucial optimization which has to be considered while designing power sources with high-power requirements. Hybrid systems with $\Lambda > 5$ show a distinct advantage over batteries in terms of energy per unit mass for high values of power densities. Where long hours of operation with low power and minimal mass are required, batteries should be preferred over the hybrid system because of the high energy density of batteries at low power density. A more rigorous way to optimize these systems would be a detailed sensitivity analysis of each parameter on the desired performance of the battery/hybrid system. This discussion of optimization (based on the selected electrochemical capacitor/battery system) focuses mainly on the operating parameters and capacitor configuration index. The parameters pertaining to the electrodes such as porosity, electrode thickness, volume fraction of the filler material, separator thickness, etc. may also be important in the optimization scheme. Rigorous analyses of these parameters in regard to the optimization of battery and electrochemical systems are presented elsewhere.[8,15,25] Obtaining analytical solutions by reducing these complex systems through judicious assumptions is a major challenge for better optimization.

Conclusions

In the present work a rigorous one-dimensional mathematical model has been developed to simulate the performance of a battery-capacitor hybrid system under pulse discharge currents. The current shared between the electrochemical capacitor and the battery has been predicted for various operating conditions such as frequency, duty ratio, and peak pulse current. The hybrid system on which the simulations are based consists of a Sony 18650 battery and Maxwell's 10F electrochemical capacitor; a complete discharge curve for this system has been simulated for pulse discharge current. Results indicate than an increase of about 6% in the run time is observed for the hybrid system over that of the battery in the case where $\upsilon = 1.0$ Hz, $\Lambda = 0.5$, and $I_p = 4.178$ A (1/3 h rate). The maximum increase in run time for fixed values of Λ and i_p has been obtained at a duty ratio $\psi \approx 0.4$ for a frequency of $\upsilon = 1.0$ Hz; this maximum occurs at lower duty ratios when the frequency of the pulse discharge current is decreased. An extensive analysis of the effect of the number of capacitors added to the battery has also been performed based on the parameter, capacitor configuration index, Λ. Finally, the power-energy relationship analyzed through Ragone plots reveals the capability of the hybrid system to deliver higher energy density than the battery-alone system while operating at high power density and high values of the configuration index.

Acknowledgments

Financial support provided by the U.S. Army Communications-Electronics Command (CECOM, contract no. DAAB07-03-3-K416) is gratefully acknowledged.

The University of South Carolina assisted in meeting the publication costs of this article.

Appendix A

Expressions used for the electrode and the transport parameters in the battery.— The active particles in the battery are assumed to be spherical and hence the active surface area to volume ratio is given by the relation

$$a_{b,j} = 3\left(\frac{1 - \varepsilon_{b,j} - \varepsilon_{b,j}^{f}}{R_b}\right), \quad j = n,p \qquad [A\text{-}1]$$

The effective diffusion coefficient of Li^+ in $LiPF_6$ is given by the Bruggeman relation

$$D_{b,j}^{eff} = D_{b,j}\varepsilon_{b,j}^{brug_{b,j}}, \quad j = n,p \qquad [A\text{-}2]$$

Similarly, the effective conductivities of Li^+ in the solid phase and the solution phase are also related by the Bruggeman coefficient

$$\sigma_{b,j}^{eff} = \sigma_{b,j}(1 - \varepsilon_{b,j} - \varepsilon_{b,j}^{f})^{brug_{b,j}}, \quad j = n,p \qquad [A\text{-}3]$$

$$\kappa_{b,j}^{eff} = \kappa_b \varepsilon_{b,j}^{brug_{b,j}}, \quad j = n,p \tag{A-4}$$

The concentration dependence of the bulk electrolyte conductivity for an electrolyte mixture of 1 M $LiPF_6$ in a 1:2 v/v mixture of EC/DMC at 25°C was fit from experimental data by Doyle et al.[26] to the following expression

$$\kappa_b = \{1.0793 \times 10^{-4} + 6.7461 \times 10^{-3} c_b - 5.2245 \times 10^{-3} c_b^2 + 1.3605 \times 10^{-3} c_b^3 - 1.1724 \times 10^{-4} c_b^4\} \tag{A-5}$$

Electrode thermodynamic data for the open-circuit potentials of the electrode materials in the battery.—The open-circuit potential of the positive electrode ($LiCoO_2$) from the Sony 18650 cell was fit to the function

$$U_j = \left\{ \frac{4.707 - 36.129\left(\frac{c_s}{c_T}\right) + 104.813\left(\frac{c_s}{c_T}\right)^2 + 149.491\left(\frac{c_s}{c_T}\right)^3 + 111.818\left(\frac{c_s}{c_T}\right)^4 - 35.705\left(\frac{c_s}{c_T}\right)^5}{1 - 7.598\left(\frac{c_s}{c_T}\right) + 21.779\left(\frac{c_s}{c_T}\right)^2 - 30.959\left(\frac{c_s}{c_T}\right)^3 + 23.632\left(\frac{c_s}{c_T}\right)^4 + 7.8474\left(\frac{c_s}{c_T}\right)^5} \right\}, \quad j = p \tag{A-6}$$

whereas for the negative electrode the experimental data was fit to the function

$$U_j = \left\{ \frac{1.997 + 2.472\left(\frac{c_s}{c_T}\right)}{1 + 31.823\left(\frac{c_s}{c_T}\right)} \right\}, \quad j = n \tag{A-7}$$

Here the ratio of the solid phase concentration to the total concentration (concentration during which the intercalation coefficient is 1) depends on the amount of lithium inserted in either electrode. The values of the intercalation coefficient obtained experimentally through slow rate discharge were 0.53 for $LiCoO_2$ and 0.9 for the carbon electrode.

Expressions used for the electrode and the transport parameters in the electrochemical capacitor.—The effective diffusion coefficient of the salt is given as

$$D_{c,j}^{eff} = D_{c,j} \varepsilon_{c,j}^{brug_{c,j}}, \quad j = n,p \tag{A-8}$$

while the effective ionic conductivity is given by the Bruggeman relation

$$\kappa_{c,j}^{eff} = \kappa_c \varepsilon_{c,j}^{brug_{c,j}}, \quad j = n,p \tag{A-9}$$

and the effective conductivity in the solid phase is given by the relation

$$\sigma_{c,j}^{eff} = \sigma_{c,j}(1 - \varepsilon_{c,j} - \varepsilon_{c,j}^{f})^{brug_{c,j}}, \quad j = n,p \tag{A-10}$$

The active carbon particles in the electrochemical capacitor are assumed to be spherical, and hence the active surface area to volume ratio is given by the relation

$$a_{c,j} = 3\left(\frac{1 - \varepsilon_{c,j} - \varepsilon_{c,i}^{f}}{R_c}\right), \quad j = n,p \tag{A-11}$$

Appendix B

Expression for the relaxation time using a simplified electrical circuit network.—An approximate time constant for the decay of the current in the battery/capacitor hybrid circuit to zero is a crucial factor in the run time extension of the hybrid system. An approximate solution for the time for the decay is obtained using a simplified circuit with the battery and a capacitor in parallel with effective internal resistances of R_b and R_c, respectively. Because the battery and the capacitor are in parallel

$$(U_{j=p} - U_{j=n}) - A_b i_b(t)\tilde{R}_b = (U_{j=p} - U_{j=n}) - A_c i_c(t)\tilde{R}_c - \frac{1}{\tilde{C}_c}\int_0^t i_c(t)dt \tag{B-1}$$

where $(U_{j=p} - U_{j=n})$ is the open-circuit potential of the battery. It is assumed that before the process of discharge the hybrid system is completely charged and has been allowed to relax for sufficient time that the open-circuit potentials across both the battery and the capacitor are the same. It is also assumed that the potential drop in the battery is purely ohmic for short time periods.

In the case when the relaxation occurs after the on time of the Nth pulse is reached, we obtain

$$A_b i_b(t) + A_c i_c(t) = 0, \quad \frac{N + \psi}{\upsilon} < t < \frac{N + 1}{\upsilon} \tag{B-2}$$

Plugging B-2 into B-1, we get a differential equation for the capacitor current

$$(\tilde{R}_b + \tilde{R}_c)\frac{d}{dt}q_c(t) + \frac{1}{\tilde{C}_c}q_c(t) = 0, \quad q_c\left(t = \frac{N + \psi}{\upsilon}\right) = \int_0^{N+\psi/\upsilon} A_c i_c(t)dt \tag{B-3}$$

Solving B-3 for $q_c(t)$ gives

$$q_c(t) = \left(\frac{\int_0^{N+\psi/\upsilon} A_c i_c(t)dt}{\exp\left(\frac{-1}{(\tilde{R}_b + \tilde{R}_c)\tilde{C}_c}\frac{N + \psi}{\upsilon}\right)} \right) \exp\left(\frac{-1}{(\tilde{R}_b + \tilde{R}_c)\tilde{C}_c}t\right) \tag{B-4}$$

Using B-4, the value of $i_c(t)$ can be calculated and after simplification yields

$$i_c(t) = i_c^{max} \exp\left(\frac{-1}{(\tilde{R}_b + \tilde{R}_c)\tilde{C}_c}(t)\right) \tag{B-5}$$

where

$$i_c^{max} = \frac{\frac{-1}{(\tilde{R}_b + \tilde{R}_c)\tilde{C}_c}\int_0^{N+\psi/\upsilon} i_c(c)dt}{\exp\left(\frac{-1}{(\tilde{R}_b + \tilde{R}_c)\tilde{C}_c}\frac{N + \psi}{\upsilon}\right)} \tag{B-6}$$

Appendix C

Two-parameter polynomial approximation for the solid phase concentration within a spherical particle.—The governing equation for transient diffusion within a solid particle is given by Eq. 6 subject to the boundary conditions

$$\frac{\partial c_{s,j}(0,t)}{\partial r} = 0, \quad j = n,p \tag{C-1}$$

$$-D_{s,j}\frac{\partial c_{s,j}(R_s,t)}{\partial r} = a_j j_{nj}, \quad j = n,p \tag{C-2}$$

The concentration profile within the spherical particle is described by a two-parameter parabolic profile and takes the form

$$c_{s,j} = C_1(t) + C_2(t)r^2 \tag{C-3}$$

where $C_1(t)$ and $C_2(t)$ are functions of time. Applying the boundary condition C-2 in C-3 and evaluating for the average concentration within the spherical particle $c_{s,j}^{ave}$ given by

$$c_{s,j}^{ave} = \int_0^{R_s} c_{s,j} 3r^2 dr \tag{C-4}$$

and integrating Eq. 6 over the particle radius

$$\int_0^{R_s} \frac{\partial c_{s,j}}{\partial t} 3r^2 dr = \int_0^{R_s} \frac{1}{r^2}\frac{\partial}{\partial r}\left[D_{s,j} r^2 \left(\frac{\partial c_{s,j}}{\partial r}\right)\right] 3r^2 dr \tag{C-5}$$

as in Ref. 17 yields the necessary differential algebraic equations to solve for the constants $C_1(t)$ and $C_2(t)$. The final equations necessary to evaluate the average concentration within the solid particle and the surface concentration are

$$\frac{\partial}{\partial t}c_{s,j}^{ave} = -3a_j j_{n,j} \tag{C-6}$$

and

$$c_{s,j}^{ave} - c_{s,j}|_{r=\hat{R}} = \frac{a_j j_{n,j} R_s}{5D_{s,j}} \tag{C-7}$$

which is derived in detail in Ref. 17.

List of Symbols

a	Specific surface area of the porous material, m^2/m^3
A	$l \times b$, area based on the dimensions of the electrode, m^2
b	height of the electrode, m
brug	Bruggeman factor

c solution phase concentration, mol/m^3
$\bar{c}$ dimensionless solution phase concentration, $(c-c^0)/c^0$
c_T concentration in intercalation material for $\Delta y = 1$, mol/m^3
c_s solid phase concentration, mol/m^3
c_s^{ave} average solid phase concentration, mol/m^3
C_1, C_2 Constants as defined in Eq. C-3
$\tilde{C}$ capacitance of the capacitor, F
C_{dl} double-layer capacitance, F/m^2
D diffusion coefficient of Li^+ in the salt, m^2/s
D_s diffusion coefficients of Li^+ in the solid phase, m^2/s
E energy of hybrid/battery system, Wh
f activity coefficient of salt
F Faraday's constant, 96487 C/equiv
i_0 exchange current density, A/m^2
$\mathbf{i_1}$ solid phase current density, A/m^2
$\mathbf{i_2}$ solution phase current density, A/m^2
I_{app} applied current, A
I_p amplitude (peak current) of the pulse profile, A
j_n reaction rate of a species in solution phase, mol/m^2/s
k intercalation reaction rate constant, m$^{5/2}$/mol$^{1/2}$/s
l electrode length when unwound (cylindrical configuration/ prismatic), m
L thickness of the cell sandwich, m
M molecular mass, g/mol
m mass of the hybrid/battery system
n number of electrons transferred in the electrode reaction
n_p number of capacitors connected in parallel to the battery
n_s number of capacitors connected in series to the battery
N number of pulses
P power of hybrid/battery system, W
q discharge capacity, A hr
$\tilde{q}$ charge density on the double-layer surface, C/m^2
r radial distance within an active material particle, m
R ideal gas constant, 8.3143 J/mol/K
R_s radius of solid spherical particles, m
$\tilde{R}$ total dc resistance of a battery/capacitor, Ω
s_i stoichiometric coefficient
t time, s
t_i^0 transference number of the ith species
T temperature, K
U open-circuit potential, V
x distance from the anode, m
$\bar{x}$ dimensionless distance, x/L
z charge number

Greek

δ thickness of anode/cathode/separator of battery/capacitor, m
ε porosity of composite electrode
η electrochemical reaction over potential, V
κ solution phase conductivity, S/m
ρ^l density of the electrolyte, kg/m^3
ρ density of the electrode material/electrolyte, kg/m^3
σ solid phase conductivity, S/m
τ run time of the battery/hybrid system, s
ψ duty ratio; ratio of the on time to the time period (1/υ) of the pulse
ξ utilization of the battery, defined in Eq. 20
υ frequency of pulse current, s^{-1}
Λ capacitor configuration index, defined in Eq. 22
λ power enhancement factor
$\bar{\upsilon}^+$ number of cations or anions into which a mole of electrolyte dissociates
Δy intercalation coefficient
ϕ_1 solid phase potential, V
ϕ_2 solution phase potential, V
τ_b time constant of the battery, s
τ_c time constant of the electrochemical capacitor, s

Subscripts

c capacitor
b battery
i species
j positive (p), negative (n) electrode for battery/capacitor
L electrolyte
ave average values
t total
T concentration in intercalation material for $\Delta y = 1$

Superscripts

0 initial condition
s separator
a anode
c Cathode
eff effective values
f filler material

References

1. B. E. Conway, *Electrochemical Supercapacitors: Scientific Fundamentals and Technological Applications*, Kluwer-Plenum, New York (1999).
2. R. Kotz and M. Carlen, *Electrochim. Acta*, **45**, 2483 (2002).
3. J. R. Miller, in *Electrochemical Capacitors*, F. M. Delnick and M. Tomkiewicz, Editors, PV 95-29, p. 246, The Electrochemical Society Proceedings Series, Pennington, NJ (1995).
4. C. E. Holland, J. W. Weidner, R. A. Dougal, and R. E. White, *J. Power Sources*, **109**, 32 (2002).
5. R. A. Dougal, S. Liu, and R. E. White, *IEEE Trans. Compon., Hybrids, Manuf. Technol.*, **25**, 120 (2002).
6. F. A. Posey and T. Morozumi, *J. Electrochem. Soc.*, **113**, 176 (1966).
7. B. Pillay and J. Newman, *J. Electrochem. Soc.*, **143**, 1806 (1996).
8. V. Srinivasan and J. W. Weidner, *J. Electrochem. Soc.*, **146**, 1650 (1999).
9. C. Lin, J. A. Ritter, B. N. Popov, and R. E. White, *J. Electrochem. Soc.*, **146**, 3168 (1999).
10. H. Kim and B. N. Popov, *J. Electrochem. Soc.*, **150**, A1153 (2003).
11. J. Newman and C. W. Tobias, *J. Electrochem. Soc.*, **109**, 1183 (1962).
12. P. DeVidts and R. E. White, *J. Electrochem. Soc.*, **144**, 1343 (1997).
13. J. S. Newman, *Electrochemical Systems*, p. 268, Prentice-Hall, Englewood Cliffs, NJ (1991).
14. M. Doyle, T. F. Fuller, and J. Newman, *J. Electrochem. Soc.*, **140**, 1526 (1993).
15. T. F. Fuller, M. Doyle, and J. Newman, *J. Electrochem. Soc.*, **141**, 1 (1994).
16. I. J. Ong and J. Newman, *J. Electrochem. Soc.*, **148**, 4360 (2001).
17. C. Y. Wang, W. B. Gu, and B. Y. Liaw, *J. Electrochem. Soc.*, **145**, 3407 (1998).
18. V. Subramanian, J. Ritter, and R. E. White, *J. Electrochem. Soc.*, **148**, E444 (1999).
19. A. M. Johnson and J. Newman, *J. Electrochem. Soc.*, **118**, 510 (1971).
20. G. Sikha, B. N. Popov, and R. E. White, *J. Electrochem. Soc.*, **151**, A1104 (2004).
21. G. Sikha and B. N. Popov, *J. Power Sources*, **134**, 130 (2004).
22. R. Moshtev and B. Johnson, *J. Power Sources*, **91**, 86 (2000).
23. K. Ozawa, *Solid State Ionics*, **69**, 212 (1994).
24. A. Chu and P. Braatz, *J. Power Sources*, **112**, 236 (2002).
25. J. Newman, *J. Electrochem. Soc.*, **142**, 97 (1995).
26. M. Doyle, J. Newman, A. S. Gozdz, C. N. Schmutz, and J.-M. Tarascon, *J. Electrochem. Soc.*, **143**, 1890 (1996).
27. C. J. Ben, B. A. Boukamp, and R. A. Huggins, *J. Electrochem. Soc.*, **126**, 2258 (1979).
28. D. Dunn and J. Newman, *J. Electrochem. Soc.*, **147**, 820 (2000).